ACSNANO

www.acsnano.org

ARTICLE

High-Performance Flexible Thermoelectric Power Generator Using Laser Multiscanning Lift-Off Process

Sun Jin Kim,[†,∥] Han Eol Lee,[‡,∥] Hyeongdo Choi,[†] Yongjun Kim,[†] Ju Hyung We,[†] Ji Seon Shin,[§] Keon Jae Lee,[*,‡] and Byung Jin Cho[*,†]

[†]Department of Electrical Engineering and [‡]Department of Materials Science and Engineering, KAIST, 291 Daehak-ro, Yuseong, Daejeon 34141, Republic of Korea

[§]Tegway Co. Ltd., #711 National Nano Fab., 291 Daehak-ro, Yuseong, Daejeon 34141, Republic of Korea

Supporting Information

ABSTRACT: **Flexible thermoelectric generators (f-TEGs) are emerging as a semipermanent power source for self-powered sensors, which is an important area of research for next-generation smart network monitoring systems in the Internet-of-things era. We report in this paper a f-TEG produced by a screen-printing technique (SPT) and a laser multiscanning (LMS) lift-off process. A screen-printed TEG was fabricated on a SiO_2/a-Si/quartz substrate *via* the SPT process, and the LMS process completely separated the rigid quartz substrate from the original TEG by selective reaction of the XeCl excimer laser with the exfoliation layer (a-Si). Using these techniques, we fabricate a prototype f-TEG composed of an array of 72 TE couples that exhibits high flexibility at various bending radii, together with excellent output performance (4.78 mW/cm^2 and 20.8 mW/g at ΔT = 25 °C). There is no significant change in the device performance even under repeated bending of 8000 cycles.**

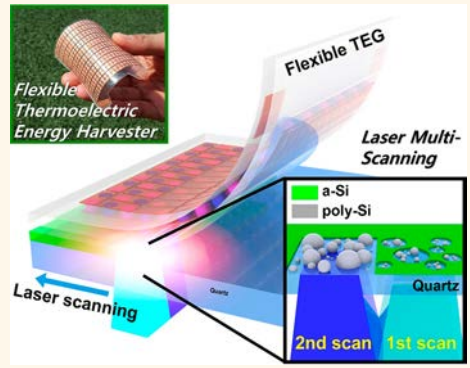

KEYWORDS: *screen-printing technique, laser multiscanning lift-off process, freestanding and flexible thermoelectric power generator*

The Internet of things (IoT) is generating a great deal of interest in relation to next-generation smart network monitoring systems. In the upcoming IoT era, autonomous sensors are expected to play an important role in a wide spectrum of applications such as medical monitoring, emergency response, and industrial and environment controls. However, it is challenging to maintain millions or even billions of sensor units widely spread in wearable systems, smart houses, smart vehicles, and industrial monitoring systems and in hard to access or dangerous locations. In this light, a self-powered and self-sustaining unit sensor system that can perform functionally independent operations without additional maintenance and changing batteries is critically important. Energy-harvesting modules such as solar cells,[1,2] vibration-based energy harvesters,[3,4] and thermoelectric generators (TEGs)[5,6] have been considered as permanent energy suppliers to unit sensor systems. Among them, the TEG is one of the promising candidates for realizing a self-powered sensor system because it contains no moving parts, thus reducing physical and electrical failure, and it is also silent and offers high reliability during long-lasting and autonomous operation. In particular, many researchers have studied the design of flexible thermoelectric generators (f-TEGs) with polymer substrates[7−9] due to their outstanding potential for using arbitrary heat source shapes without an additional heat exchanger. However, the flexible polymer substrates cause thermal energy loss and tensile/compressive strain into the active region containing the TE materials and electrodes during bending, resulting in performance degradation. Designing a freestanding f-TEG module with no substrate is hence an important task for realizing high-output performance together with high flexibility. The inorganic-based laser lift-off method has been recognized as a potential solution and offers diverse advantages for freestanding devices. This method allows rapid fabrication and high yield for manufacturing electrical devices, and it also does not cause degradation of device characteristics after separating the external substrate from the device because the laser irradiated to the device during laser lift-off reacts only with the exfoliation layer. Our research group has demonstrated a stable laser lift-off process and successfully realized a few cases of flexible electronic devices without characteristic breakdown, including flexible resistive random access memory,[10] a piezoelectric

Received: July 26, 2016
Accepted: November 17, 2016
Published: November 17, 2016

DOI: 10.1021/acsnano.6b05004
ACS Nano 2016, 10, 10851−10857

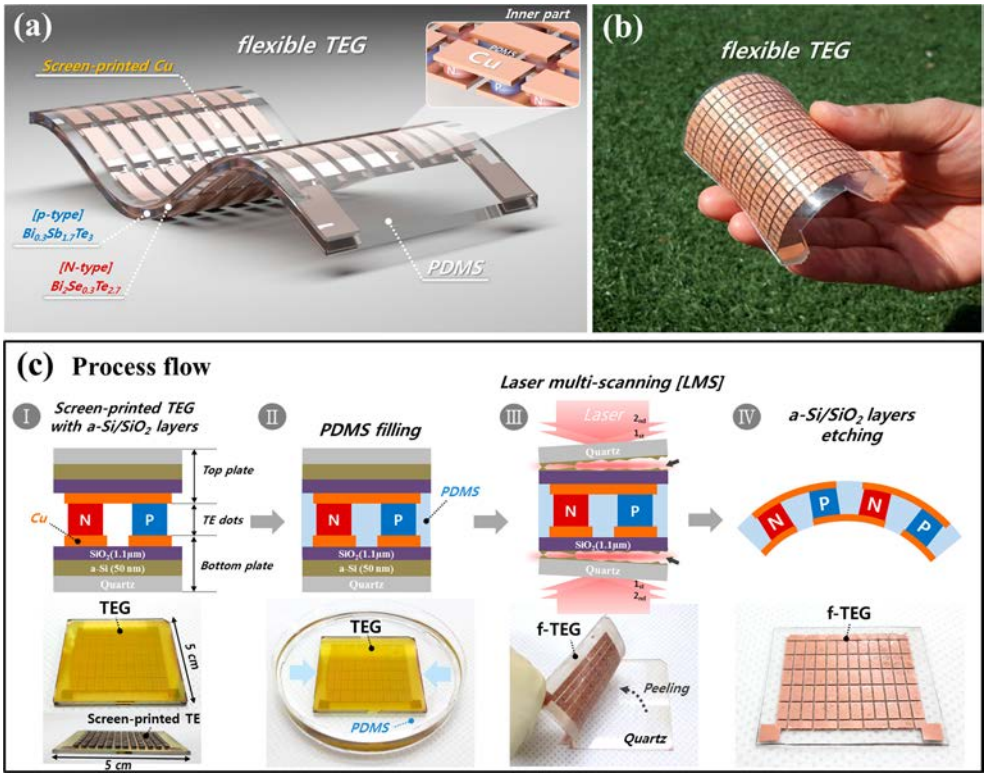

Figure 1. (a,b) Schematic illustration and actual photo of the freestanding f-TEG prepared using a LMS lift-off process. (c) Fabrication steps for a freestanding f-TEG. (c-I) Preparation of the screen-printed TEG with top and bottom substrates (SiO_2/a-Si/quartz plate). (c-II) Infiltrating the elastic polymer (PDMS) into the gap between the TE legs. (c-III) Removal of the top and bottom plates using the LMS process. (c-IV) Removing the remaining SiO_2/a-Si layers by etching in a diluted mixture of hydrogen fluoride and hydrochloric acid.

energy harvester,[11] and an acoustic nanosensor.[12] In light of these results, the laser lift-off transfer process has garnered attention in the flexible electronics field and plays a key role for self-powered sensor systems by resolving major issues.

In this paper, we propose a method to fabricate a high-performance f-TEG using a screen-printing technique (SPT) and a laser multiscanning (LMS) lift-off process. A f-TEG containing inorganic TE materials (p-type $Bi_{0.3}Sb_{1.7}Te_3$ film and n-type $Bi_2Se_{0.3}Te_{2.7}$ film) is fabricated on SiO_2/a-Si/quartz wafer by a SPT process, and multiple irradiation scanning of a XeCl excimer laser through the back side of the quartz substrate is implemented to detach the screen-printed TEG from the rigid quartz substrates. A prototype integrating an array of 72 thermoelectric (TE) couples is fabricated and evaluated. The freestanding f-TEG module not only shows higher output power density of 4.78 mW/cm^2 at ΔT = 25 °C but also presents excellent flexibility and mechanical stability with a smaller bending radius down to 5 mm and negligible degradation under repeated bending of 8000 cycles, compared to a previous study.[13]

RESULTS AND DISCUSSION

Process Integration for Fabricating a Freestanding f-TEG. In order to realize a freestanding f-TEG without a substrate, we fabricated a TEG using SPT and LMS processes. Figure 1a presents an image of the f-TEG device, illustrating the internal structure of the device in detail. The curvy and deformable f-TEG contains screen-printed TE thick films (p-type $Bi_{0.3}Sb_{1.7}Te_3$, n-type $Bi_2Se_{0.3}Te_{2.7}$), which are connected electrically in series with Cu electrodes and thermally in parallel as a traditional bulk-type TEG structure. The ambient between the TE thick films is filled with an elastic polymer (polydimethylsiloxane, PDMS) to increase flexibility and prevent damage from oxidation and mechanical impact. Figure 1b shows a photo of the 4 in. scale f-TEG developed in this work.

The fabrication steps for the freestanding f-TEG are illustrated in Figure 1c, with actual device photos. The integration process begins with fabricating a screen-printed TEG on a SiO_2 (1.1 μm)/a-Si (50 nm)/quartz substrate (Figure 1c-I). Here, the amorphous silicon (a-Si:H) layer deposited by plasma-enhanced chemical vapor deposition (PECVD) with a mixture gas of SiH_4/H_2 at a temperature of 300 °C is used as an exfoliation layer that helps to separate the completed f-TEG from the rigid quartz substrate by laser irradiation at the end of this fabrication process. The SiO_2 layer is also deposited by PECVD using SiH_4/N_2O at a temperature of 300 °C after the a-Si:H deposition to protect the device layer by compensating thermal and mechanical stress during the LMS process. The screen-printed Cu film is printed on the top and bottom plates and then annealed for crystallization and densification. Meanwhile, we fabricate an array of screen-printed TE films on a quartz plate by a SPT process. Formation of the screen-printed TE thick films is shown in Figure S1. Each TE thick film has a diameter of 2 mm and a thickness of 650 μm, which is a suitable dimension for both high flexibility and power density and reproducibility of the TEG device. Large dimension of the TE film causes poor flexibility, while low TE dimension can lead to weak mechanical property and high contact resistance as well as a difficult fabrication process. In this trade-off, we have chosen TE legs with a diameter 2 mm and a thickness of 650 μm, which can provide both reasonably

DOI: 10.1021/acsnano.6b05004
ACS Nano 2016, 10, 10851−10857

good flexibility and power density and reproducibility of the TEG device. Moreover, circle-type TE films are preferred because of the advantage in mechanical stress upon bending. Thermoelectric properties of the screen-printed $Bi_{0.3}Sb_{1.7}Te_3$ (p-type) and $Bi_2Se_{0.3}Te_{2.7}$ (n-type) thick films are shown in Table S1. The screen-printed TE thick films have electrical conductivity lower than that of the bulk TE materials due to the porosity of the screen-printed TE films, as shown in Figure S2. However, the thermal conductivity of the film is also lower compared to that of the bulk TE materials because of the same reason. The pores electrically and thermally restrict the carrier and phonon transport in the screen-printed TE films. As there is a trade-off relationship between the electrical and thermal properties, the screen-printed TE films still have quite reasonable ZT values of 0.80 (p-type) and 0.49 (n-type). A 2 μm thick Ni layer is next deposited on both sides of the TE films as an interfacial layer between the TE film and Cu electrode. The Ni layer is deposited by sputtering because a high-purity Ni layer is required to reduce contact resistance. Except the Ni layer, all other layers in the device such as p-type and n-type TE materials, Cu electrodes, and soldering materials are formed by the screen-printing process. The array of TE films on the quartz substrate is transferred onto the top and bottom plates and then bonded together using a solder paste. The sample is then dipped into PDMS to fill the gap (~650 μm) between the top and bottom plates with an elastic polymer, followed by a hardening process at 90 °C for 40 min (Figure 1c-II). The two rigid quartz plates are then simply peeled off from the f-TEG immediately after the LMS process (Figure 1c-III). Further information on the LMS process can be found in Figures 2 and 3. In the next step, we remove the

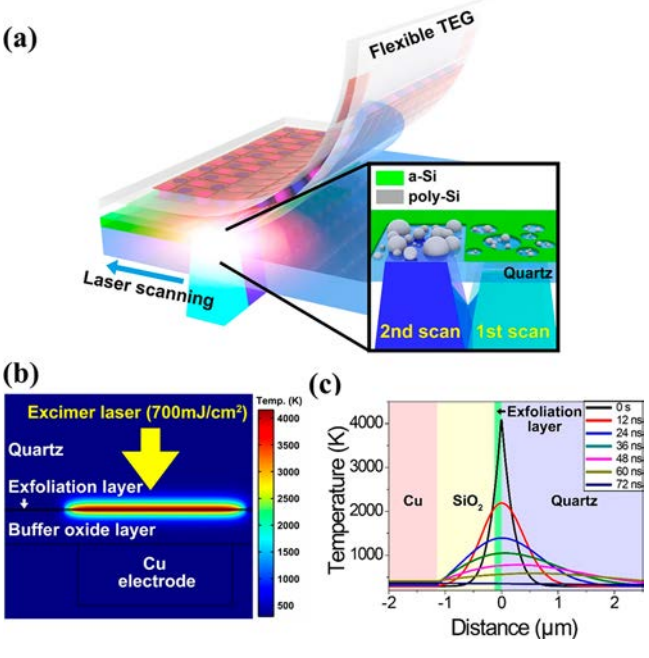

Figure 2. FEM simulation results when the two consecutive UV-excimer lasers with a high energy density of 700 mJ/cm^2 and a pulse frequency of 20 Hz are irradiated to the a-Si layer through the backside of the quartz substrate. (a) Schematic illustrations of the laser lift-off process based on LMS exfoliation for the f-TEG. The inset displays the detailed surface state after each laser scanning. (b) Temperature distribution and (c) thermal profile as a function of the *z* axis of the overall device.

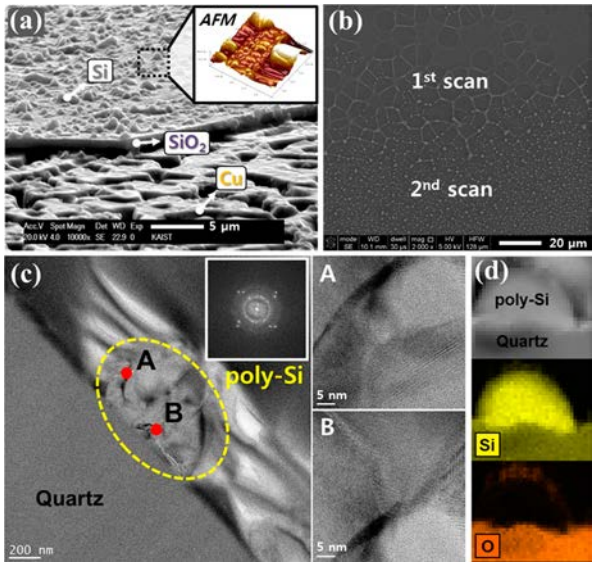

Figure 3. (a) Tilted SEM image of the f-TEG surface after the LMS exfoliation process. The top inset shows AFM mapping results of Si hillocks on the buffer oxide layer. (b) SEM image of the a-Si layer on the quartz substrate after UV-laser irradiation once (the top side of image) and twice (the bottom side of image). (c) TEM image of a Si nanoparticle formed on the quartz mother substrate. The upper inset shows the fast Fourier transform pattern of the Si lattice. The cross-sectional high-resolution TEM images display a poly-Si lattice and grain boundary near the surface (A), and the center (B) of the Si nanoparticle. (d) High-angle annular dark-field TEM image of a Si nanoparticle and EDS elemental mapping results of Si and O.

remaining SiO_2/a-Si layers by etching them in a diluted mixture of hydrogen fluoride and hydrochloric acid (Figure 1c-IV) and then finally achieve a freestanding f-TEG that is thin (~800 μm), light (~0.24 g/cm^2), and flexible. A photo of an actual f-TEG with dimensions of 40 mm × 40 mm × 0.8 mm is presented in Figure 1c-IV.

Theoretical Interpretation of the LMS Exfoliation Process *via* Finite Element Method Simulation. Various flexible electronic devices (*e.g.*, resistive memory,[10] nanogenerator,[11] and acoustic sensor[12]) have been successfully realized *via* inorganic-based laser lift-off (ILLO). Although the ILLO process is well-established with a fast, stable, and large-scale exfoliation technique, the device fabrication temperature was restricted to about 500 °C before a XeCl excimer laser irradiation step because high fabrication temperature accelerated dehydration of the exfoliation layer (a-Si:H). The dehydration of the exfoliation layer (a-Si:H) can lead to failure in delamination of the device layer during XeCl excimer laser of 500 mJ/cm^2 because of the lack of hydrogen which provides energy for the separation of the layers.[14] In current work, the hydrogen release from the a-Si:H layer was unavoidable because a high-temperature annealing process (>700 °C) must be done to recrystallize Cu electrodes printed on a SiO_2/a-Si:H/quartz substrate (see Figures S4 and S5). Thus, the previous exfoliation method described in ref 10 was not successful for fabricating a flexible TEG. To overcome this limitation, we applied a LMS exfoliation process with a higher laser energy density of 700 mJ/cm^2 and a pulse frequency of 20 Hz. The multiple laser irradiations could fully react with the dehydrated exfoliation layer (a-Si), resulting in the agglomeration of a-Si layer, and then completely delaminate the flexible TEG device layer with no thermal damage. Our approach using

DOI: 10.1021/acsnano.6b05004
ACS Nano 2016, 10, 10851−10857

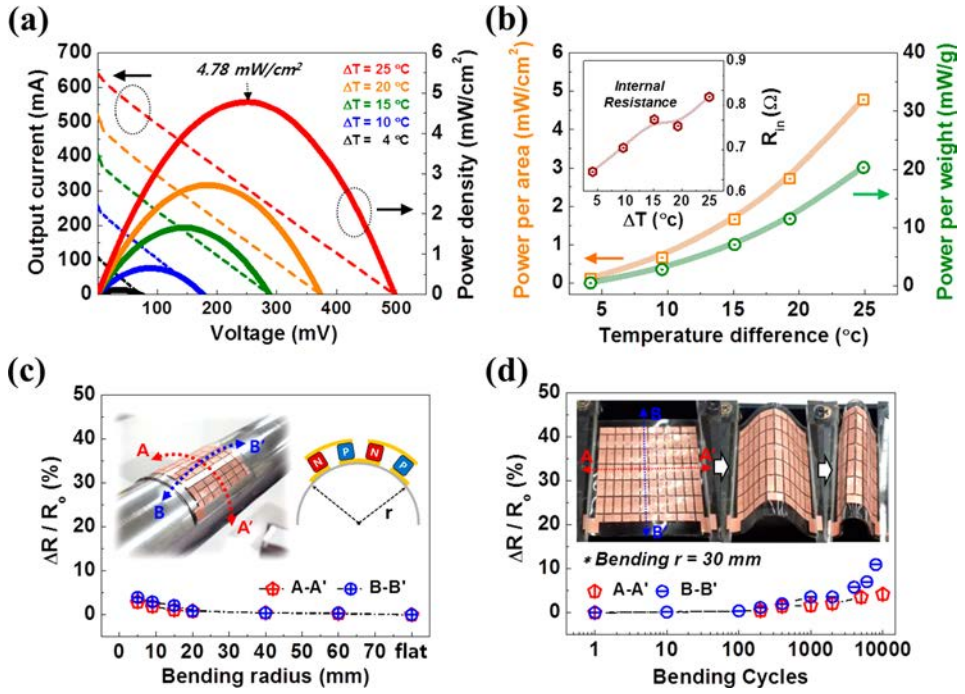

Figure 4. Output characteristics of the freestanding f-TEG (72 TE couples). (a) Current–voltage (I–V) curves (dashed lines) and output power density (thick lines) with respect to ΔT. (b) Output power per unit area (open square) and unit weight (open circle). The inset shows the change of internal resistance with respect to ΔT. (c) Internal resistance stability under bending stress along both horizontal (A–A′) and vertical (B–B′) directions, as illustrated in the inset. (d) Durability test through multiple strain cycles with a bending radius of 30 mm. The inset shows photographs of the f-TEG in the flat state and the bending state.

the laser multiscanning process allows us to use a high-temperature annealing process over 700 °C during device fabrication processes, which is an important advance because high-performance device fabrication often requires a high-temperature process. Figure 2a provides a schematic illustration of the LMS lift-off process, depicting magnified images of the laser-irradiated area in the inset. To exfoliate a high-temperature-annealed TEG array from a sacrificial quartz substrate, a pulsed UV-excimer laser, which is widely used in high-end display industries for sequential lateral solidification and excimer laser annealing,[15,16] was exposed several times from the backside of a transparent quartz substrate and interacted with a dehydrated amorphous silicon (a-Si) exfoliation layer. The top TEG layers were detached from the bulk quartz substrate by the reduced adhesion between the exfoliation layer and the quartz mother substrate. Unlike the general ILLO process, because the UV-excimer laser was irradiated to the optical-reactive layer several times during the LMS exfoliation process, the temperature of the device layers can be increased over thousands of Kelvin with thermal damage.[17]

To protect the TEG array from laser-induced damage, prior to actual application of the LMS process, we theoretically calculated the thermal distribution by a finite element method (FEM) simulation. Figure 2b presents the calculated temperature distribution by the heat transfer mode of FEM after the two consecutive laser irradiations with a high energy density of 700 mJ/cm^2 and a pulse frequency of 20 Hz. According to the FEM simulation results, the flexible TEG array still can be protected from thermal damage by using the 1.1 μm thick buffer oxide layer even after harsher laser irradiation of the LMS compared to that of the previously published ILLO process.[18] Figure 2c shows the calculated temperature profile of the entire TEG device on the quartz substrate after the LMS process. After two irradiations of the excimer laser, the temperature of the a-Si layer increased immediately to 4151 K, and it then cooled by conductive heat flux toward the surface of the quartz mother substrate. After 72 ns, the entire TEG device was cooled to room temperature. These results indicate that the LMS lift-off process can be exploited to realize a large-scale flexible TEG without significant thermal damage.

Material Characterizations of Exfoliation Layer after Multiscanning LLO. The ILLO process is a sophisticated exfoliation technique that can be used to fabricate flexible electronic devices. Heretofore, the mechanism of the general ILLO process has been explained by melting,[11] disassembly,[19] and vaporization[20] of an exfoliation layer. However, there is no interpretation of the LMS exfoliation process using an exfoliation layer that was previously annealed over 700 °C. To clearly analyze the peel-off phenomenon in the LMS lift-off process, we experimentally investigated the separate side of the exfoliation layer. Figure 3a shows a tilted scanning electron microscope (SEM) image of the flexible TEG surface after the LMS process. In the SEM image, there are many nanoscale Si hillocks on the top surface. As shown in the inset of Figure 3a, the surface of the Si nanostructures was analyzed by an atomic force microscope (AFM). The detached side of the a-Si layer has a comparatively uniform surface with a root-mean-square (R_{rms}) of 4.239 nm and an arithmetic average (R_a) of 4.529 nm. Figure 3b displays a SEM image that shows different results after the first and second laser scanning. As the UV-excimer laser was irradiated to the exfoliation layer, some Si nanoparticles (NPs) and microscale holes randomly formed on the surface of the laser-reactive layer. Additional laser scanning then completely transformed the a-Si layer to numerous Si NPs. In-depth analyses of the Si NPs were performed by transmission electron microscopy (TEM),

DOI: 10.1021/acsnano.6b05004
ACS Nano 2016, 10, 10851–10857

energy-dispersive spectroscopy (EDS), and time-of-flight secondary ion mass spectroscopy (TOF-SIMS). Figure 3c presents a cross-sectional TEM image of a Si NP on the quartz substrate. Its high-resolution TEM images show a polycrystalline Si lattice near the surface (A) and the center (B) of the Si NP. The fast Fourier transform pattern in the inset of Figure 3c also proves that the laser-induced Si NPs are in a polycrystalline phase. The results of EDS element mapping and TOF-SIMS reveal that a Si NP is composed entirely of Si, as presented in Figure 3d and Figure S4. According to the analysis results, it appears that numerous Si NPs were likely created to decrease the higher Gibbs free energy by interaction with the UV-excimer laser.[21] Therefore, we concluded that the Si NPs produced the LMS exfoliation phenomena by minimizing the surface contact area between the TEG device and the quartz mother substrate.[22]

Output Characteristics of the Freestanding f-TEG. A prototype f-TEG comprising 72 TE couples of $Bi_{0.3}Sb_{1.7}Te_3$ (p-type) and $Bi_2Se_{0.3}Te_{2.7}$ (n-type) films with a size of 40 mm × 40 mm × 0.8 mm was fabricated. Evaluation of the output characteristics was carried out with a computer-controlled multimeter and sourcemeter. To generate a temperature difference (ΔT) across the f-TEG, a heating and cooling system was set up, as shown in Figure S8a. Once the temperature difference across the device is in a thermally steady-state mode, the voltage−current characteristics are simultaneously measured as a function of the input voltage and then translated to a power curve at a certain ΔT. Actual temperature at the hot and cold sides was monitored during the test, as shown in Figure S8b. The actual temperatures of both the hot and cold sides simultaneously increase as ΔT increases because the heat transfer occurs from the hot side to the cold side through the thin TEG device. Figure 4a presents the voltage−current curve (dash lines) and the output power density (thick lines) with respect to ΔT. During the measurement time, a steep current drop was found at the beginning of the input voltage. This is because the thermal energy is delivered to the cold side by the charge carriers flowing under a short-circuit-like condition (Peltier effect), causing a smaller ΔT and a lower electrical potential across the TE legs. Furthermore, it was found that the internal resistance increases together with ΔT (the inset of Figure 4b) because the f-TEG was subjected to more thermal and mechanical stress at a large ΔT. In Figure 3d, the open-circuit voltage is 500 mV, and the power generated is about 4.78 mW/cm^2 at ΔT = 25 °C. The f-TEG device with a weight of 3.7 g generates the power per unit weight of 20.8 mW/g at ΔT = 25 °C. The lightweight is attributed to high porosity of the screen-printed TE films[23,24] and an optimal TEG structure without a supporting substrate. Average power densities divided by ΔT^2 are about 7.3 μW/cm^2·K^2 and 30.8 μW/g·K^2 which are 5-fold and 3-fold greater than those of the previously reported TEG fabricated on a glass fabric (1.4 μW/cm^2·K^2 and 10.4 μW/g·K^2), respectively. Key features underlying these improvements are the use of ternary TE materials with a high ZT as the raw materials of the screen-printed TE film and a significant reduction of the contact resistance between the TE film and solder material using the Sn-based solder paste instead of Ag paste.

Device Characteristics under Bending Stress. In order to investigate the device reliability under mechanical stress, we monitored the change of internal resistance after bending with various bending radii and through multiple strain cycles along both horizontal (A−A′) and vertical (B−B′) directions (Figure 4c,d). The two bending directions and radius are defined in the inset of Figure 4c. The generator, which has internal resistance of 0.5 Ω, was tested with a bending radius of down to 5 mm, and the impedance variation was simultaneously measured by utilizing an alternating current pulse (delta function) with a high frequency in order to suppress the Peltier effect (Figure 4c). This indicates that there was no significant change (less than 5%) in the internal resistance, whereas the resistance along the vertical direction (B−B′) increases slightly faster than that along the horizontal direction (A−A′). For a durability test, the generator was repeatedly bent up to 10 000 cycles with a bending radius of 30 mm. The f-TEG device also exhibits stable internal resistance (less than 5%) up to 10 000 cycles along the horizontal direction but shows noticeable degradation in the vertical direction at over 8000 cycles, and device breakdown occurs after around 10 000 cycles. The asymmetry in reliability along these directions originates from the asymmetric array of Cu electrodes, as shown in the actual photo of the device (Figure 4d). Under a bended situation, the Cu electrodes on the outer surface are under strong tensile stress in the vertical bending test (B−B′), but the mechanical stress is mostly concentrated on the elastic polymer matrix (PDMS) in the horizontal bending test (A−A′). Therefore, it is important to reduce mechanical stress on the Cu electrode by using the elastic polymer matrix and carefully designing a symmetric device configuration for a highly flexible and foldable TE generator. Drop testing on granite floor tiles was performed to demonstrate mechanical stability of the device (Figure S9). In order to engineer the flexibility of the device, we can control the TE leg dimension and the packing density (area ratio between the printed TE region and space region). Easiest way to enhance flexibility of the device is to reduce the packing density of the device. However, this will lead to the reduction of the generated power per area. In the device with a very low packing density, the flexibility is limited by the flexibility of the copper electrode and the filler polymer. If we keep the packing density constant but still want to enhance the flexibility, smaller dimension TE legs must be used with high level integration. Then, total series resistance will increase and the fabrication process becomes more difficult. There is a trade-off relationship between flexibility and device performance. The resistance curve shows no noticeable damage on the freestanding device up to a height of 3 m (less than 2%) because the polymer matrix containing TE films plays a role of a shock absorber upon drop impact. The high softness of the TE generator would be a strong benefit for applications involving severe vibration stress, such as in vehicles and industrial facilities.

CONCLUSION

In summary, previously reported f-TEGs had a low power density caused by low TE material properties and non-optimal device structure as well as problems related to production such as long processing time and lab-scale fabrication. The method to fabricate a high-performance f-TEG presented in this paper, using SPT and LMS processes, can overcome the aforementioned limitations. The processes are well-known for being cheaper and faster than sputtering,[25] evaporation,[26] and electrochemical[27] processes and offer better scalability for large-area applications. The capability of printing TE materials on a very large area without a sophisticated lithography patterning process and forming TE films of several hundred micrometers thickness *via* the SPT process is critical in terms of

DOI: 10.1021/acsnano.6b05004
ACS Nano 2016, 10, 10851−10857

achieving high-performance f-TEG. In addition, the LMS process can successfully separate the external substrate from the original device without degradation of the device performance thanks to the selective reaction of the XeCl excimer laser with the exfoliation layer (a-Si). The prototype composed of an array of 72 TE couples shows outstanding power generation performance (4.78 mW/cm^2 and 20.8 mW/g at ΔT = 25 °C), flexibility, and durability upon repeated bending cycles. The output power density surpasses the best performance reported to date for curvy and deformable TEGs.[28−31] The approach described in this work would be highly beneficial for commercializing freestanding devices and provides a way of fabricating the f-TEG module.

MATERIALS AND METHODS

Formation of $Bi_{0.3}Sb_{1.7}Te_3$ (p-Type) and $Bi_2Se_{0.3}Te_{2.7}$ (n-Type) Thick Films. Formation of the screen-printed TE thick films is described in Supporting Information. The commercial bulk-type TE materials were used as the starting materials. The bulk ingot was crashed into powders using a planetary ball miller. The powder size was controlled by the ball milling time and the speed of revolution. After the ball milling process, the TE paste was synthesized by mixing TE powder, an organic binder, and a solvent. The TE paste was then printed on a ceramic substrate. The printed film was dried on a hot plate for volatilization of the organic solvent. Here, the TE printing and drying processes were repeatedly conducted to meet the target TE thickness (~700 μm). $Bi_{0.3}Sb_{1.7}Te_3$ (p-type) and $Bi_2Se_{0.3}Te_{2.7}$ (n-type) thick films finally underwent an annealing process.

Experimental Setup for the Laser Multiscanning Process. The LMS process was carried out with a XeCl excimer laser (a wavelength of 308 nm). The excimer laser is released from a combination of xenon and chlorine gas under suitable conditions of high pressure and 22 kV extraction voltage. During the LMS process, laser shots with a high energy density of 700 mJ/cm^2 were irradiated to the exfoliation layer with a frequency of 20 Hz and a time duration of 30 ns, and the exfoliation layer was scanned twice in a "S" shape.

Output Characteristics Measurement of the f-TEG. To evaluate the output power density of the f-TEG, we set up a heating and cooling system with a Keithley 2425 sourcemeter and a Keithley 2700 multimeter, which extract the output voltage *versus* current curve and monitor the actual temperature at the hot and cold sides of the f-TEG device. The f-TEG was embedded with ceramic paste between the temperature-controlled Al blocks in the system. Ceramic paste was applied to the top and bottom sides of the f-TEG to electrically insulate the bare Cu electrodes and also effectively transfer heat to the generator. Thin thermocouples were placed at the hot and cold sides of the f-TEG to carefully measure the temperature gradient across the device. The temperature of the cold side was relatively fixed at roughly 300 K by using a cooling water system. A temperature difference ranging from 0 to 25 °C could be obtained by increasing the hot side temperature using a heating controller. In a thermally steady state mode at a certain ΔT, the output current was measured as a function of the input voltage by a Keithley 2425 sourcemeter, and ΔT across the device was monitored by a Keithley 2700 multimeter. The power density at various ΔT was then calculated from the measured $I-V$ curve. In addition, the internal resistance of the f-TEG was measured using the Keithley 2425. To minimize the Peltier effect, we utilized an alternating current pulse (delta function) with high frequency (20 Hz) and then calculated the average resistance from multiple analyses.

Modeling and Simulation. In Figure 2b, the simulation results of the temperature distribution were calculated by the heat transfer mode of a FEM simulation (COMSOL Multiphysics 4.4 software). The heat flux and distribution of the overall film are calculated from the following heat transfer equation:

$$\rho C\frac{\partial T}{\partial t} - \nabla\cdot(k\Delta T) = Q \quad (1)$$

where ρ is the density of a specific material, T is the temperature, C is the thermal capacity, k is the thermal conductivity, t is the time, and Q is the heat flux. Density (ρ = 2259 kg/m^3), thermal capacity (C = 700 J/kg·K), and heat conductivity (k = 1.3 W/m·K) of the a-Si thin film were substituted into the model.[32,33] Furthermore, the optical characteristic parameters of a-Si at a wavelength of 308 nm were considered to calculate the temperature distribution: the absorption (α = 1.12 × 10^{6}1/cm) and reflection coefficient (R = 0.305), which were measured by a UV spectrometer (Shimadzu Co., UV3101pc). The entire structure of the f-TEG and quartz substrate was defined to be analogous to the actual structure.

ASSOCIATED CONTENT

Supporting Information

The Supporting Information is available free of charge on the ACS Publications website at DOI: 10.1021/acsnano.6b05004.

Figures S1−S9 and Table S1 (PDF)

AUTHOR INFORMATION

Corresponding Authors

*E-mail: keonlee@kaist.ac.kr. Tel: +82-42-350-3343. Fax: +82-42-350-3310.

*E-mail: bjcho@kaist.edu. Tel: +82-42-350-3485. Fax: +82-42-350-8565.

ORCID

Byung Jin Cho: 0000-0003-3000-5403

Author Contributions

‖S.J.K. and H.E.L. contributed equally to this work.

Notes

The authors declare no competing financial interest.

ACKNOWLEDGMENTS

This work was supported by the National Research Foundation of Korea (NRF) grant funded by the Korean Government (MSIP) (NRF-2015R1A5A1036133).

REFERENCES

(1) Kim, B.-J.; Kim, D. H.; Lee, Y.-Y.; Shin, H.-W.; Han, G. S.; Hong, J. S.; Mahmood, K.; Ahn, T. K.; Joo, Y.-C.; Hong, K. S.; Park, N.-G.; Lee, S.; Jung, H. S. Highly Efficient and Bending Durable Perovskite Solar Cells: Toward a Wearable Power Source. *Energy Environ. Sci.* **2015**, *8*, 916−921.

(2) Yoon, J.; Baca, A. J.; Park, S. I.; Elvikis, P.; Geddes, J. B.; Li, L. F.; Kim, R. H.; Xiao, J. L.; Wang, S. D.; Kim, T. H.; Motala, M. J.; Ahn, B. Y.; Duoss, E. B.; Lewis, J. A.; Nuzzo, R. G.; Ferreira, P. M.; Huang, Y. G.; Rockett, A.; Rogers, J. A. Ultrathin Silicon Solar Microcells for Semitransparent, Mechanically Flexible and Microconcentrator Module Designs. *Nat. Mater.* **2008**, *7*, 907−915.

(3) Seol, M.-L.; Woo, J.-H.; Jeon, S.-B.; Kim, D.; Park, S.-J.; Hur, J.; Choi, Y.-K. Vertically Stacked Thin Triboelectric Nanogenerator for Wind Energy Harvesting. *Nano Energy* **2015**, *14*, 201−208.

(4) Wang, Z. L.; Chen, J.; Lin, L. Progress in Triboelectric Nanogenerators as a New Energy Technology and Self-Powered Sensors. *Energy Environ. Sci.* **2015**, *8*, 2250−2282.

(5) Khan, Q. A.; Bang, S. J. Energy Harvesting for Self Powered Wearable Health Monitoring System. *Oregon State University* **2009**, 11−15.

(6) Leonov, V.; Vullers, R. J. Wearable Electronics Self-Powered by using Human Body Heat: The State of the Art and the Perspective. *J. Renewable Sustainable Energy* **2009**, *1*, 062701.

(7) Suemori, K.; Hoshino, S.; Kamata, T. Flexible and Lightweight Thermoelectric Generators Composed of Carbon Nanotube−Polystyrene Composites Printed on Film Substrate. *Appl. Phys. Lett.* **2013**, *103*, 153902.

(8) Francioso, L.; De Pascali, C.; Farella, I.; Martucci, C.; Cretì, P.; Siciliano, P.; Perrone, A. Flexible Thermoelectric Generator for Wearable Biometric Sensors. *Proceedings of the IEEE Sensors 2010 Conference*; Waikoloa, HI, November 1−4, 2010; IEEE: New York, 2010; pp 747−750.
(9) Lu, Z.; Layani, M.; Zhao, X.; Tan, L. P.; Sun, T.; Fan, S.; Yan, Q.; Magdassi, S.; Hng, H. H. Fabrication of Flexible Thermoelectric Thin Film Devices by Inkjet Printing. *Small* **2014**, *10*, 3551−3554.
(10) Kim, S.; Son, J. H.; Lee, S. H.; You, B. K.; Park, K.-I.; Lee, H. K.; Byun, M.; Lee, K. J. Flexible Crossbar-Structured Resistive Memory Arrays on Plastic Substrates *via* Inorganic-Based Laser Lift-Off. *Adv. Mater.* **2014**, *26*, 7480−7487.
(11) Park, K.-I.; Son, J. H.; Hwang, G.-T.; Jeong, C. K.; Ryu, J.; Koo, M.; Choi, I.; Lee, S. H.; Byun, M.; Wang, Z. L.; Lee, K. J. Highly-Efficient, Flexible Piezoelectric PZT Thin Film Nanogenerator on Plastic Substrates. *Adv. Mater.* **2014**, *26*, 2514−2520.
(12) Lee, H. S.; Chung, J.; Hwang, G.-T.; Jeong, C. K.; Jung, Y.; Kwak, J.-H.; Kang, H.; Byun, M.; Kim, W. D.; Hur, S.; Oh, S.-H.; Lee, K. J. Flexible Inorganic Piezoelectric Acoustic Nanosensors for Biomimetic Artificial Hair Cells. *Adv. Funct. Mater.* **2014**, *24*, 6914−6921.
(13) Kim, S. J.; We, J. H.; Cho, B. J. A Wearable Thermoelectric Generator Fabricated on a Glass Fabric. *Energy Environ. Sci.* **2014**, *7*, 1959−1965.
(14) Serin, T.; Serin, N.; Tarimci, Ç.; Ünal, B. Determination of Thermal Annealing Effect in Intrinsic a-Si:H Film. *J. Non-Cryst. Solids* **2000**, *276*, 163−168.
(15) Kim, M.; Jin, G.; Kim, K. B.; Song, J. Effects of the Single and Double (Overlap) Scanned Excimer Laser Annealing on Solid Phase Crystallized Silicon Films. *Displays* **2015**, *36*, 9−12.
(16) Carta, F.; Gates, S. M.; Limanov, A. B.; Im, J. S.; Edelstein, D. C.; Kymissis, I. Sequential Lateral Solidification of Silicon Thin Films on Cu BEOL-Integrated Wafers for Monolithic 3-D Integration. *IEEE Trans. Electron Devices* **2015**, *62*, 3887−3891.
(17) Thompson, M. O.; Galvin, G. J.; Mayer, J. W.; Peercy, P. S.; Poate, J. M.; Jacobson, D. C.; Cullis, A. G.; Chew, N. G. Melting Temperature and Explosive Crystallization of Amorphous Silicon during Pulsed Laser Irradiation. *Phys. Rev. Lett.* **1984**, *52*, 2360.
(18) Pecora, A.; Maiolo, L.; Cuscunà, M.; Simeone, D.; Minotti, A.; Mariucci, L.; Fortunato, G. Low-Temperature Polysilicon Thin Film Transistors on Polyimide Substrates for Electronics on Plastic. *Solid-State Electron.* **2008**, *52*, 348−352.
(19) Li, K. Y.; Tai, N. H.; Lin, I. N. Preparation of PNN-PZT Thick Film on Pt/Ti/SiO_2/Si Substrate by Laser Lift-Off Process. *Integr. Ferroelectr.* **2005**, *69*, 135−141.
(20) Ueda, T.; Ishida, M.; Yuri, M. Separation of Thin GaN from Sapphire by Laser Lift-Off Technique. *Jpn. J. Appl. Phys.* **2011**, *50*, 041001−041006.
(21) Herlach, D. M.; Feuerbacher, B. Non-Equilibrium Solidification of Undercooled Metallic Melts. *Adv. Space Res.* **1991**, *11*, 255−262.
(22) Pastewka, L.; Robbins, M. O. Contact between Rough Surfaces and a Criterion for Macroscopic Adhesion. *Proc. Natl. Acad. Sci. U. S. A.* **2014**, *111*, 3298−3303.
(23) We, J. H.; Kim, S. J.; Kim, G. S.; Cho, B. J. Improvement of Thermoelectric Properties of Screen-Printed Bi_2Te_3 Thick Film by Optimization of the Annealing Process. *J. Alloys Compd.* **2013**, *552*, 107−110.
(24) Kim, S. J.; We, J. H.; Kim, J. S.; Kim, G. S.; Cho, B. J. Thermoelectric Properties of P-type Sb_2Te_3 Thick Film Processed by a Screen-Printing Technique and a Subsequent Annealing Process. *J. Alloys Compd.* **2014**, *582*, 177−180.
(25) Zheng, Z. H.; Fan, P.; Luo, J. T.; Cai, X. M.; Liang, G. X.; Zhang, D. P.; Ye, F. Thermoelectric Properties of Bismuth Antimony Tellurium Thin Films Through Bilayer Annealing Prepared by Ion Beam Sputtering Deposition. *Thin Solid Films* **2014**, *562*, 181−184.
(26) Takashiri, M.; Kurita, K.; Hagino, H.; Tanaka, S.; Miyazaki, K. Enhanced Thermoelectric Properties of Phase-Separating Bismuth Selenium Telluride Thin Films *via* a Two-Step Method. *J. Appl. Phys.* **2015**, *118*, 065301.
(27) Snyder, G. J.; Lim, J. R.; Huang, C. K.; Fleurial, J. P. Thermoelectric Microdevice Fabricated by a MEMS-Like Electrochemical Process. *Nat. Mater.* **2003**, *2*, 528−531.
(28) Glatz, W.; Schwyter, E.; Durrer, L.; Hierold, C. Bi_2Te_3 -Based Flexible Micro Thermoelectric Generator with Optimized Design. *J. Microelectromech. Syst.* **2009**, *18*, 763−772.
(29) Finefrock, S. W.; Zhu, X.; Sun, Y.; Wu, Y. Flexible Prototype Thermoelectric Devices Based on Ag_2Te and PEDOT: PSS Coated Nylon Fibre. *Nanoscale* **2015**, *7*, 5598−5602.
(30) Kim, M. K.; Kim, M. S.; Lee, S.; Kim, C.; Kim, Y. J. Wearable Thermoelectric Generator for Harvesting Human Body Heat Energy. *Smart Mater. Struct.* **2014**, *23*, 105002.
(31) Toshima, N.; Oshima, K.; Anno, H.; Nishinaka, T.; Ichikawa, S.; Iwata, A.; Shiraishi, Y. Novel Hybrid Organic Thermoelectric Materials:Three-Component Hybrid Films Consisting of a Nanoparticle Polymer Complex, Carbon Nanotubes, and Vinyl Polymer. *Adv. Mater.* **2015**, *27*, 2246−2251.
(32) Renner, O.; Zemek, J. Density of Amorphous Silicon Films. *Czech. J. Phys.* **1973**, *23*, 1273−1276.
(33) Cahill, D. G.; Katiyar, M.; Abelson, J. R. Thermal Conductivity of a-Si: H Thin Films. *Phys. Rev. B: Condens. Matter Mater. Phys.* **1994**, *50*, 6077−6082.

DOI: 10.1021/acsnano.6b05004
ACS Nano 2016, 10, 10851−10857